



Design of a broadband achromatic dielectric metasurface for linear polarization in the near-infrared spectrum

ZIJING ZHANG,¹ ZHICHEN CUI,¹ YUAN LIU,¹ SICHENG WANG,¹
ISABELLE STAUDE,² ZHENYU YANG,^{1,3} and MING ZHAO^{1,4}

¹School of Optical and Electronic Information, Huazhong University of Science and Technology, 430074 Wuhan, China

²Institute of Applied Physics, Abbe Center of Photonics, Friedrich Schiller University Jena, 07745 Jena, Germany

³zyang@mail.hust.edu.cn

⁴zhaoming@mail.hust.edu.cn

Abstract: The elimination of broadband chromatic aberrations is a crucial factor for focusing lenses. Conventional refractive glass lenses are bulky, unwieldy, and eradicating their chromatic dispersion is complicated. Dielectric metasurfaces represent a promising alternative due to their ultra-thin, ultra-compact, single-layer, and planar profile on the order of the wavelength or below. Here, we design an achromatic dielectric metasurface for linear polarization that achieves continuous focusing performance over an ultra-broad band from $1.31\mu\text{m}$ to $1.55\mu\text{m}$. The metasurface consists of a single layer of elliptic Si nanocylinders with different radii meticulously designed for an accurate manipulation of the phase profile. The focal length remains constant with a less than 1.6% alternation over the entire operation bandwidth (compared with 9.4% alternation of a chromatic metasurface). The high NA (0.36), high focal efficiency (average over 50%), and small FWHM all corroborate the excellent focusing performance of our metasurface. Furthermore, the continuous broadband focusing performance is preserved under oblique incidence (10° angle) with a stable focal length. The designed metasurface offers important opportunities for applications in linear polarized optics, fiber sensors, laser scanning fluorescence microscopy, optical signal transmission, and integrated on-chip devices in the forthcoming future.

© 2018 Optical Society of America under the terms of the [OSA Open Access Publishing Agreement](#)

1. Introduction

Conventional optical components for focusing are usually based on refractive glass lenses, and are limited by their bulky size, unwieldiness, and, crucially, large chromatic aberrations for a wide operating bandwidth. The chromatic dispersion causes a broadening of optical signal pulses, thereby limiting the capacity of optical data transmission channels. To eliminate chromatic aberrations, the optical system is bound to be more ponderous and complicated.

With the recent emergence of optical metasurfaces [1–4], a new approach to realize focusing lens components became available, which relies on direct and precise manipulation of the optical phase by nanostructured thin films. Utilizing subwavelength-spaced structures with a thickness at the wavelength scale or below, converging metasurface lenses offering overwhelming advantages over traditional refractive optical lenses can be realized. For example, their ultra-thin and planar profile allows for flexible and versatile applications, their compact and miniaturized dimensions enable portable and wearable usage, and chromatic and monochromatic dispersion can be easily eliminated without requiring complex compound structures. During the last few years we have witnessed a surge of research leading to the development of metasurfaces providing a large range of functionalities, such as metasurface polarimeters [5–7], axicons [8], and holograms [9,10], or even metasurfaces for computational imaging [11]. However, the large chromatic aberrations in these previous

systems have been a critical obstacle for achieving enhanced imaging quality. Substantial efforts were made to tackle this problem, leading to the demonstration of achromatic imaging in several discrete wavelengths [12–14]. However, in order to eliminate chromatic dispersion continuously over a broad operation band, addressing only several discrete wavelengths is insufficient. Thus, more recently, several broadband achromatic metaleenses operating in versatile wavelengths have been realized [15–21]. However, many broadband metaleenses are limited to circularly polarized incident light, which restricts the flexibility of their application to some extent. Or some broadband metaleenses [15] are polarization insensitive and can't distinguish or detect the polarization state. As such, a design for a broadband achromatic metasurface lens typically for linear input polarization in the near-IR spectral range is still missing. Regarding the potential use of metasurface lenses in future applications, their capability to operate specially with linearly polarized light is highly desirable, as it avoids the need for complex preconditioning of the input field.

Here, we design an achromatic dielectric metalens operating in the near-IR spectral range for linear input polarization. The designed achromatic metalens is theoretically analyzed based on comprehensive numerical calculations using the finite-difference time-domain (FDTD) method. We demonstrate that the focal length remains constant over a broad bandwidth spanning at least 240nm from 1.31 μm to 1.55 μm . The focusing quality is tested under vertical and oblique incidence. The focal distance stays constant at around 38.8 μm with less than 1.6% alternation (compared with a chromatic metalens showing 9.4% alternation) in the operating bandwidth. Furthermore, the continuous broadband focusing performance is preserved under oblique incidence (10° angle) with a stable focal length over the entire spectral operation band. The near-IR spectrum ranging from 1.31 μm to 1.55 μm is critical for optical communication. By conquering the broadband chromatic aberration, the metalens can be a promising component for focusing, collimating, Wavelength Division Multiplexing (WDM), coupling and beam shaping.

2. Principle and design

Accurate control of the phase as a function of spatial position and wavelength is key to a broadband achromatic metalens that can precisely focus light with different wavelengths to the same point. The basic general equation for the phase value is given by [22]:

$$\varphi(r, f) = -\frac{2\pi f}{c}(\sqrt{r^2 + F^2} - F) + \varphi(0, f) \quad (1)$$

where r is the spatial distance from the center of the metalens, f is the frequency of incident light, c is the speed of light, and F is the designed focal length. Meanwhile, $\varphi(0, f)$ is the central phase value that can be initially decided freely. For a single wavelength focusing metalens, one merely needs to abide by the above equation [23]. However, for a broadband achromatic metalens design, the phase profile should be observed in a large bandwidth. We can decompose the phase equation by a Taylor expansion to see the phase change for different frequency:

$$\varphi(r, f) = \sum_{n=0}^{\infty} \frac{\Phi(r, f_c)^{(n)}}{n!} (f - f_c)^{(n)} \quad (2)$$

Here, f_c is the central frequency, $\varphi(r, f_c)^{(n)}$ is the n -th partial derivative of $\varphi(r, f)$ at $f = f_c$. If the phase $\varphi(r, f)$ created by the metalens is not a linear function of frequency f , it is difficult to estimate if the phase $\varphi(r, f)$ satisfies Eq. (1). Therefore, here we restrict the discussion to the case that $\varphi(r, f)$ is a linear function of f . The first term of Eq. (1) is a linear function of f , and the second term $\varphi(0, f)$ must also be a linear function of f . Thus, we get the following equations from Eq. (2):

$$\frac{\partial^n}{\partial f^n} \varphi(r, f) = 0 \quad n \geq 2 \quad (3)$$

$$\frac{\partial \varphi(r, f)}{\partial f} = -\frac{2\pi f}{c} (\sqrt{r^2 + F^2} - F) + \frac{\partial \varphi(0, f)}{\partial f} \quad (4)$$

$$\varphi(r, f) = \varphi(r, f_c) + (f - f_c) \frac{\partial}{\partial f} \varphi(r, f_c) \quad (5)$$

The $\frac{\partial}{\partial f} \varphi(0, f_c)$ is the initial dispersion index value at the center of the metalens. By controlling the central frequency phase $\varphi(r, f_c)$ and dispersion index value $\frac{\partial}{\partial f} \varphi(r, f_c)$ simultaneously, the phase manipulation can meet the focusing requirement in a continuous wavelength range. To attain an achromatic broadband metalens, we should fulfill the range of dispersion index value at each designated central frequency phase concurrently, which means that the central frequency phase $\varphi(r, f_c)$ and dispersion index value $\frac{\partial}{\partial f} \varphi(r, f_c)$ must satisfy the following equations after we have confirmed the central frequency phase $\varphi(0, f_c)$ and dispersion index value $\frac{\partial}{\partial f} \varphi(0, f_c)$ at $r = 0$ from Eqs. (1), (4), and (5):

$$\varphi(r, f_c) - \varphi(0, f_c) = -\frac{2\pi f_c}{c} (\sqrt{r^2 + F^2} - F) + 2\pi m \quad (6)$$

$$\frac{\partial}{\partial f} \varphi(r, f_c) - \frac{\partial}{\partial f} \varphi(0, f_c) = -\frac{2\pi}{c} (\sqrt{r^2 + F^2} - F) \quad (7)$$

Here, m is an arbitrary integer. For circular polarized light, the central frequency phase $\varphi(r, f_c)$ can be manipulated independently from the dispersion index $\frac{\partial}{\partial f} \varphi(r, f_c)$ by changing the rotation angle [17]. However, for linear polarized light as considered in this work, the two parameters cannot be isolated by an independent design parameter like rotation. Hence, we need to find the nanostructure parameters that satisfy the two conditions at the same time.

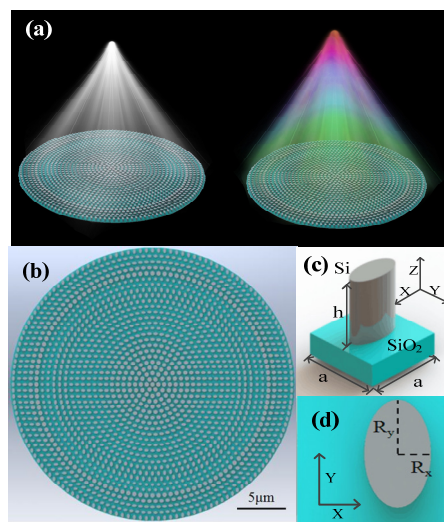


Fig. 1. (a) An artist's impression of an achromatic metalens with a constant focal point for different wavelengths (left) and of a chromatic metalens whose focal point depends on the wavelength. Schematic of (b) the metalens design and (c,d) of an individual elliptical cylinder-shaped nanostructure (oblique and top view, respectively).

The schematics of an achromatic metalens that can converge the light for a broad spectrum of wavelengths into one focal point and a chromatic metalens that will cause the change of focal point for different wavelengths are presented in Fig. 1(a). The metalens consists of numerous radial-arrayed nanostructures. Each nanostructure is an elliptical silicon pillar situated on a silica substrate, as shown in Fig. 1(b)–1(d). The reason to choose silicon is that the material possesses a transparency window ($k = 0$) for wavelength longer than 1 μm , a high refractive index for strong light-matter interaction, and a weak chromatic dispersion from 1.31 μm to 1.55 μm that can lead to an excellent linear relationship between phase and frequency. The silicon nanostructures all have a height of 600 nm. The lattice constant is $a = 600\text{nm}$. By altering the long axis and short axis of each nanostructure, we can flexibly change the phase profile on the basis of interfacial phase discontinuity [24]. The phase variation can cover the whole $0\text{--}2\pi$ and more. Meanwhile, the phase dispersion index is observed and calculated, too. The nanostructure can be interpreted as a miniaturized waveguide. When the geometric parameters R_x and R_y change, the waveguide dispersion and modal dispersion (caused by different modes excited in the waveguide) will correspondingly change [25]. So the dispersion index of different geometric parameters varies, too.

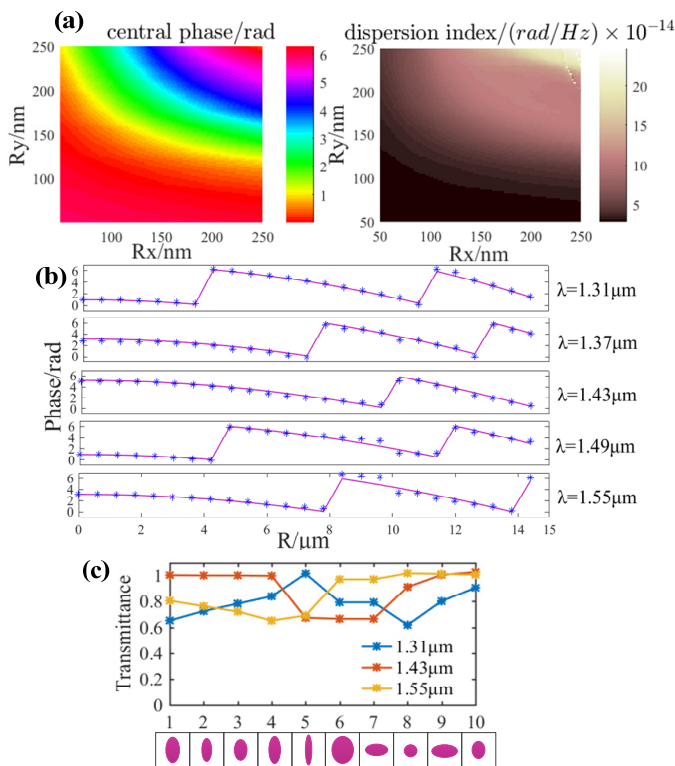


Fig. 2. (a) The library of different nanostructures. The dispersion index (left) and central phase (right) should simultaneously meet the Eqs. (5), (6), and (7). (b) Ideal phase profile (purple lines) and simulated phase profile of each nanostructure (blue asterisks) as a function of distance R from the metalens center for five wavelengths spanning the operation band. (c) Exemplary transmittance of 10 nanostructures out of 25 kinds in total for three different wavelengths.

The simulation of each nanostructure and of the final metalens is realized by a commercial software (FDTD solutions). The incident plane wave propagates along the Z-axis with polarization along the X-axis. The boundary conditions for the calculation of the whole metalens are set to PML (perfectly matched layer) in all directions. For simulations of individual nanostructures, periodic boundary conditions are applied in X- and Y-direction to account for their periodic arrangement. First, to obtain the phase and dispersion data of different nanostructures, we set up a library with different R_x and R_y values ($101 \times 101 = 10201$) as shown in Fig. 2(a), and filter the library with customized algorithms. The chosen nanostructures (25 kinds in total) have exactly the required central frequency phase as well as the dispersion index value. Every nanostructure's parameters have been listed in [Data File 1](#). The local phase of the nanostructures at different radii for different wavelengths is presented in Fig. 2(b). The required phase value (purple line) and the chosen nanostructure's phase value (orange rhombus) are in excellent agreement. The transmittance of the 10 different nanostructures used to construct the metalens is shown in Fig. 2(c). The transmittance is defined as the ratio of light intensity transmitted by a single nanostructure to the incident light intensity.

3. Results and discussion

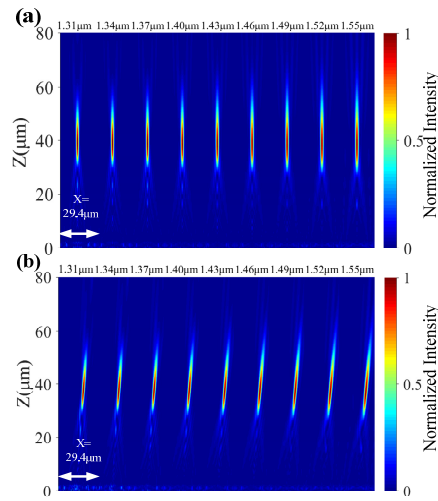


Fig. 3. Normalized intensity distributions of the achromatic metalens along axial planes under normally incident plane wave (a) and oblique incident (incidence angle 10°) plane wave (b) illumination for nine wavelengths spanning the operation band.

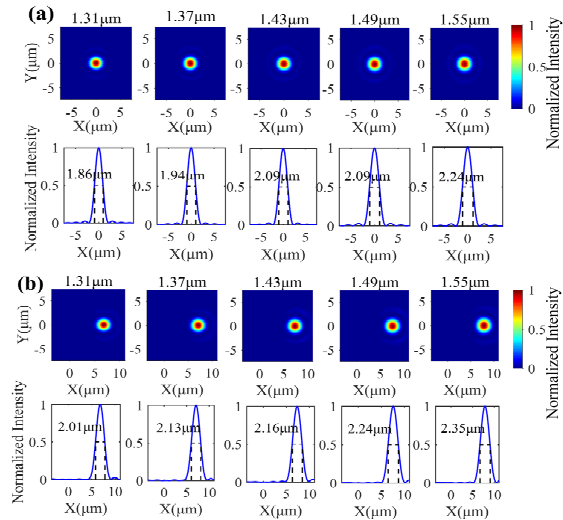


Fig. 4. Transverse focal spots profiles (top row) and normalized intensity distributions with an indication of the FWHM (bottom row) under normal incidence plane wave (a) and oblique incidence (incidence angle 10°) plane wave (b) illumination for five different wavelengths spanning the operation bandwidth.

The focusing performances of our designed broadband achromatic metalens was simulated based on the FDTD method. To confirm the effectiveness of our achromatic design, the quality of the metasurface was tested for normally incident light, as well as for oblique incident light with 10° incidence angle. The calculated intensity distributions along axial planes illuminated by a normally incident and an oblique plane wave are shown in Fig. 3(a) and Fig. 3(b) respectively. To verify the broadband achromatic performance of the metasurface over the entire designed bandwidth, we present the intensity profiles along the x-z planes for nine closely spaced wavelengths. As the series of figures clearly indicates, the light transmitted by the metalens is strongly focused at the same position over the whole tuning

bandwidth. No evident deformation or distortion of the beam shape is observed neither for normal incidence nor for oblique incidence, confirming the success of our design. Furthermore, the focusing characteristics of the focal spots are provided in Fig. 4. Transverse focal spots profiles and normalized intensity distributions with an indication of the full width at half-maximum (FWHM) irradiated by a normal plane wave and an oblique plane wave are separately presented in Fig. 4(a) and Fig. 4(b). As expected, the light energy is intensively concentrated at the same point across the large near-IR spectrum for normal as well as oblique incidence. An average FWHM of $2.04\mu\text{m}$ is achieved for normal incidence and $2.17\mu\text{m}$ for oblique incidence. Furthermore, another significant focusing performance metrics, the focusing efficiency, which is defined as the light intensity ratio in the FWHM of the focal point to the whole light intensity in the focal plane, was calculated nine different wavelengths spanning the operation bandwidth. The focusing efficiency ranges from 55.53% to 50.07% (λ from $1.31\mu\text{m}$ to $1.55\mu\text{m}$), with an average of 52.95%.

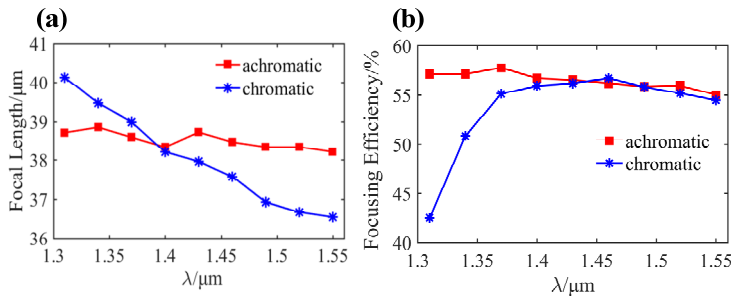


Fig. 5. Comparison of the focal length (a) and focal efficiency (b) between the achromatic metalens design (red squares) and its chromatic counterpart (blue asterisks).

To substantiate that the chromatic aberration is soundly corrected, we also design a chromatic metalens that has an identical focal distance with the achromatic counterpart at a single wavelength ($\lambda = 1.4\mu\text{m}$) only. Each nanostructure is chosen to possess the designated phase value at $\lambda = 1.4\mu\text{m}$, but the dispersion index isn't designed by us intentionally. Every nanostructure's parameters have been listed in [Data File 1](#). From Fig. 2(a), we could get the conclusion that one central phase φ may correspond to several different dispersion index. Here we use the notation $N(\varphi)$ to represent a set of dispersion index, and every element of the set is the dispersion index that the central phase φ corresponds to. So for one designed central phase φ , we can select the dispersion index from the set $N(\varphi)$ randomly for generalization. The chromatic metalens can still have a focusing capacity over the wideband, but the focal distance varies largely. The contrast of focal distance shift in the operating bandwidth is presented in Fig. 5(a). As the figure shows, the focal length of the chromatic metalens has an alternation of $3.58\mu\text{m}$ (9.4% to the average focal length) over the entire bandwidth, while the focal length of the achromatic metalens only exhibits a maximum alternation of $0.64\mu\text{m}$ (1.6% to the average focal length). Another significant imaging performance metrics is the focusing efficiency, which is defined in this letter as the light intensity ratio in the FWHM of the focal point to the whole light intensity in the focal plane. The focusing efficiencies of achromatic metalens and chromatic metalens are presented in Fig. 5(b). As the curves demonstrate, the achromatic metalens has a high average focal efficiency over 50%. In contrast, the chromatic metalens has a sharp attenuation of focal efficiency when the wavelength decreases and the average focal efficiency is relatively smaller as compared to the achromatic design.

4. Conclusion

In summary, a continuous broadband (240nm) achromatic dielectric metalens for near-IR wavelengths and linear polarization has been proposed and numerically demonstrated in this

letter. We theoretically develop a design principle to manipulate the phase of a single wavelength and the range of the dispersion index. The simulated phase profile shows an excellent agreement with the required phase profile. An almost constant focal distance as well as diffraction-limited focusing performance is achieved over the entire operation band and even for oblique incidence, no distortions of the focus is evident, pointing towards a good imaging performance of the designed metalens. For prospective enhancement, more degrees of freedom can be introduced to augment the accessible range of dispersion index, such as cascading layers, doublet or triplet nanostructures, different heights of nanostructures, or combinations of heterogeneous materials. By employing a variety of design factors, achromatic metalenses with larger diameter, higher NA, and broader spectrum can be realized.

Funding

National Natural Science Foundation of China (NSFC) (61475058); Fundamental Research Funds for the Central Universities (HUST, 2017KFYXJJ025); Open Fund of the State Key Laboratory of High Performance Complex Manufacturing (Kfkt2016-10).

References

1. N. Yu and F. Capasso, "Flat optics with designer metasurfaces," *Nat. Mater.* **13**(2), 139–150 (2014).
2. A. V. Kildishev, A. Boltasseva, and V. M. Shalaev, "Planar photonics with metasurfaces," *Science* **339**(6125), 1232009 (2013).
3. K. Huang, F. Qin, H. Liu, H. Ye, C. W. Qiu, M. Hong, B. Luk'yanchuk, and J. Teng, "Planar diffractive lenses: fundamentals, functionalities, and applications," *Adv. Mater.* **30**(26), 1704556 (2018).
4. A. Arbabi, Y. Horie, A. J. Ball, M. Bagheri, and A. Faraon, "Subwavelength-thick lenses with high numerical apertures and large efficiency based on high-contrast metasurfaces," *Nat. Commun.* **6**(1), 7069 (2015).
5. J. P. Balthasar Mueller, K. Leosson, and F. Capasso, "Ultracompact metasurface in-line polarimeter," *Optica* **3**(1), 42 (2016).
6. A. Pors, M. G. Nielsen, and S. I. Bozhevolnyi, "Plasmonic metagratings for simultaneous determination of Stokes parameters," *Optica* **2**(8), 716 (2015).
7. S. Wei, Z. Yang, and M. Zhao, "Design of ultracompact polarimeters based on dielectric metasurfaces," *Opt. Lett.* **42**(8), 1580–1583 (2017).
8. D. Lin, P. Fan, E. Hasman, and M. L. Brongersma, "Dielectric gradient metasurface optical elements," *Science* **345**(6194), 298–302 (2014).
9. K. Huang, Z. Dong, S. Mei, L. Zhang, Y. Liu, H. Liu, H. Zhu, J. Teng, B. Luk'yanchuk, J. K. W. Yang, and C.-W. Qiu, "Silicon multi-meta-holograms for the broadband visible light," *Laser Photonics Rev.* **10**(3), 500–509 (2016).
10. X. Li, L. Chen, Y. Li, X. Zhang, M. Pu, Z. Zhao, X. Ma, Y. Wang, M. Hong, and X. Luo, "Multicolor 3D metaholography by broadband plasmonic modulation," *Sci. Adv.* **2**(11), e1601102 (2016).
11. S. Colburn, A. Zhan, and A. Majumdar, "Metasurface optics for full-color computational imaging," *Sci. Adv.* **4**(2), eaar2114 (2018).
12. F. Aieta, M. A. Kats, P. Genevet, and F. Capasso, "Multiwavelength achromatic metasurfaces by dispersive phase compensation," *Science* **347**(6228), 1342–1345 (2015).
13. M. Khorasaninejad, F. Aieta, P. Kanhaiya, M. A. Kats, P. Genevet, D. Rousso, and F. Capasso, "Achromatic Metasurface Lens at Telecommunication Wavelengths," *Nano Lett.* **15**(8), 5358–5362 (2015).
14. M. Khorasaninejad, A. Y. Zhu, C. Roques-Carmes, W. T. Chen, J. Oh, I. Mishra, R. C. Devlin, and F. Capasso, "Polarization-Insensitive Metalenses at Visible Wavelengths," *Nano Lett.* **16**(11), 7229–7234 (2016).
15. M. Khorasaninejad, Z. Shi, A. Y. Zhu, W. T. Chen, V. Sanjeev, A. Zaidi, and F. Capasso, "Achromatic Metalens over 60 nm Bandwidth in the Visible and Metalens with Reverse Chromatic Dispersion," *Nano Lett.* **17**(3), 1819–1824 (2017).
16. S. Wang, P. C. Wu, V. C. Su, Y. C. Lai, M. K. Chen, H. Y. Kuo, B. H. Chen, Y. H. Chen, T. T. Huang, J. H. Wang, R. M. Lin, C. H. Kuan, T. Li, Z. Wang, S. Zhu, and D. P. Tsai, "A broadband achromatic metasurface in the visible," *Nat. Nanotechnol.* **13**(3), 227–232 (2018).
17. W. T. Chen, A. Y. Zhu, V. Sanjeev, M. Khorasaninejad, Z. Shi, E. Lee, and F. Capasso, "A broadband achromatic metasurface for focusing and imaging in the visible," *Nat. Nanotechnol.* **13**(3), 220–226 (2018).
18. A. Arbabi, E. Arbabi, S. M. Kamali, Y. Horie, S. Han, and A. Faraon, "Miniature optical planar camera based on a wide-angle metasurface doublet corrected for monochromatic aberrations," *Nat. Commun.* **7**, 13682 (2016).
19. E. Arbabi, A. Arbabi, S. M. Kamali, Y. Horie, and A. Faraon, "Controlling the sign of chromatic dispersion in diffractive optics with dielectric metasurfaces," *Optica* **4**(6), 625–632 (2017).
20. S. Wang, J. Lai, T. Wu, C. Chen, and J. Sun, "Wide-band achromatic flat focusing lens based on all-dielectric subwavelength metasurface," *Opt. Express* **25**(6), 7121–7130 (2017).

21. S. Wang, P. C. Wu, V. C. Su, Y. C. Lai, C. Hung Chu, J. W. Chen, S. H. Lu, J. Chen, B. Xu, C. H. Kuan, T. Li, S. Zhu, and D. P. Tsai, "Broadband achromatic optical metasurface devices," *Nat. Commun.* **8**(1), 187 (2017).
22. F. Aieta, P. Genevet, M. A. Kats, N. Yu, R. Blanchard, Z. Gaburro, and F. Capasso, "Aberration-free ultrathin flat lenses and axicons at telecom wavelengths based on plasmonic metasurfaces," *Nano Lett.* **12**(9), 4932–4936 (2012).
23. M. Khorasaninejad, W. T. Chen, R. C. Devlin, J. Oh, A. Y. Zhu, and F. Capasso, "Metalenses at visible wavelengths: Diffraction-limited focusing and subwavelength resolution imaging," *Science* **352**(6290), 1190–1194 (2016).
24. N. Yu, P. Genevet, M. A. Kats, F. Aieta, J. P. Tetienne, F. Capasso, and Z. Gaburro, "Light propagation with phase discontinuities: generalized laws of reflection and refraction," *Science* **334**(6054), 333–337 (2011).
25. Y. Li, X. Li, M. Pu, Z. Zhao, X. Ma, Y. Wang, and X. Luo, "Achromatic flat optical components via compensation between structure and material dispersions," *Sci. Rep.* **6**(1), 19885 (2016).